^{18}F-FDG-PET

Prior to baseline ^{18}F-FDG PET scanning, all subjects fasted for at least 4 h. Intravenous administration of ^{18}F-FDG (254 ± 107 MBq) was followed by a resting period of 40–60 min in a dimly-lit and quiet room, where participants were instructed to keep their eyes open. A static scan for 10.3 ± 5.5 min was performed in 2D or 3D mode after the resting period. Attenuation was corrected by a transmission scan with segmentation for dedicated PET and by a CT scan for PET/CT. Supplementary Table 2 lists the PET and PET/CT devices and reconstruction conditions.

The ^{18}F-FDG PET images were processed with the 3-dimensional stereotactic surface projections (3D-SSP) technique to generate z-score maps, using iSSP software version 3.5 (Nihon Medi-Physics Co. Ltd., Tokyo, Japan). The normal database used for generating the z-score maps was constructed based on 50 normal subjects (31 males and 19 females, average age = 57.6 y), with 10 normal subjects each from 5 participating institutions. The healthy subjects for the normal database had no memory complaint and no history of neurologic or psychiatric disorders. The results of their neurologic examination and brain imaging examinations (MR imaging or CT) were normal, and their cognitive function was judged to be normal by experienced neurologists (MMSE score, 25–30).

PET image interpretation

Three experts, blinded to clinical information, independently assessed the reconstructed PET images, referring to the 3D-SSP z-score map and correlating with MRI to classify the images into different dementia patterns of P1-P3, P1+, and N1-N3 [15]. When evaluations of the three raters did not completely match, the cases were discussed, and a consensus reading was agreed upon.

PET score

We calculated the AD t-sum, as described in previous publications [16, 17], by using the procedure implemented as module PALZ in the PMOD software package (version 3.2; PMOD Technologies, Zurich, Switzerland). The AD t-sum indicates the severity of the metabolic decrease in those brain areas that are typically affected by AD (multimodal association cortices mostly located in the temporal and parietal lobes), including an adjustment for an age effect.

In the present study, the AD t-sum was converted into the PET score by reference to its upper limit of normal, as determined previously [16], and log transformation to approach a normal distribution of values, according to the following equation [18]: PET score = log2 {(AD t-sum/11089)+1}.

MRI

All the subjects were scanned with a 1.5 T or 3T MRI system. A T1-weighted fast field echo sequence was used. Supplementary Table 3 lists the MRI devices and reconstruction conditions. T1-weighted 3-dimensional sagittal sections of the brains were acquired and analyzed on a PC using a voxel-based specific regional analysis system for Alzheimer's disease (VSRAD® advance, Eisai Co, Ltd, Tokyo, Japan), which was developed based on the voxel-based morphometry method and is now freely available [19–23]. First, equalization of voxel sizes and linear and nonlinear transformations were performed. Next, images of gray matter, white matter, and cerebrospinal fluid were separated, and the gray matter images were standardized and smoothed onto templates by using DARTEL (Wellcome Department of Imaging Neuroscience, London, UK). By using the z-score analysis method, comparative statistical analysis of the voxels was performed for the healthy control database. The database for the healthy controls contained data from 40 men and 40 women, each aged 54–86 (mean 70.2 ± 7.3) years. In this study, the averaged positive z-score in the target volume of interest (VOI) for the medial temporal structure, including the entorhinal cortex, head to tail of the hippocampus, and amygdala was used for further analyses.

Follow-up

Patients were observed at 1-year intervals for 3 years. The CDR, MMSE, EMCL, and WMS-R-LM were re-administered at each visit. Repeat ^{18}F-FDG-PET and MRI scans were optional. The ADAS-J cog was also administered as an option in selected centers. Conversion to dementia was established when the CDR became ≥1.0. No further follow-up of patients after reaching CDR ≥1.0 was requested. AD was diagnosed in a given center when a patient fulfilled both CDR ≥1.0 and the National Institute of Neurological and Communicative Disorders–Alzheimer's Disease and Related Disorders Association's (NINCDS-ADRDA) "probable AD" criteria. The diagnosis of other causes was based on established clinical criteria for each disease, including vascular dementia (VaD) [23], dementia with Lewy bodies (DLB) [25], frontotemporal dementia (FTD) [26], and Creutzfeldt–Jacob disease [27].

Researchers (YW and YA) of the study group, who were highly experienced in evaluating dementia, finalized the clinical outcome of each case based on the submitted case report form. They were blinded as to the PET results.

Logistic regression analysis

Multivariate logistic regression analyses were used to assess whether baseline ^{18}F-FDG-PET was predictive of longitudinal clinical outcome. We estimated the odds of AD converters versus non-converters as a function of age, gender, education level, WMS-R-LM II, and PET score. Results were considered significant at $p < 0.05$. Statistical analyses were performed using SPSS (version 14.0; SPSS Inc., Chicago, IL) for Windows (Microsoft).

RESULTS

Baseline characteristics and neuropsychologic reevaluation

In total, 114 patients (64 women and 50 men; mean age, 70.8 ± 7.5) were included in the study. The mean education level was 11.5 ± 3.0 years. Of these 114 patients, 23 withdrew from the study, including 5 with no follow-up, 5 with only 1 visit, and 13 with 2 visits without conversion to dementia. Because of the uncertainty concerning their cognitive status over time, these 23 patients were excluded from the outcome analyses. Of the remaining 91 subjects, 44 patients progressed to dementia, 41 developed AD, and 3 developed non-AD dementia (FTD, DLB, and VaD) (Fig. 1). The patterns of PET images for those 3 patients were as follows: FTD patient, P2; DLB and VaD patients, P1. Since AD was the primary outcome of the study, the patients with non-AD dementia were excluded from further analyses and were not considered in the denominator for the analysis of prediction accuracy. The cumulative conversion rate over 3 years was 47%.

Demographic and neuropsychological data at the initial visit in patients who developed AD (AD-converters) and those who did not (non-converters) are shown in Table 1. At baseline, the two groups differed in the MMSE, ADAS-J cog, WMS-R-LM, and GDS scores. There was no difference observed in age, educational level, or gender distribution between these two groups.

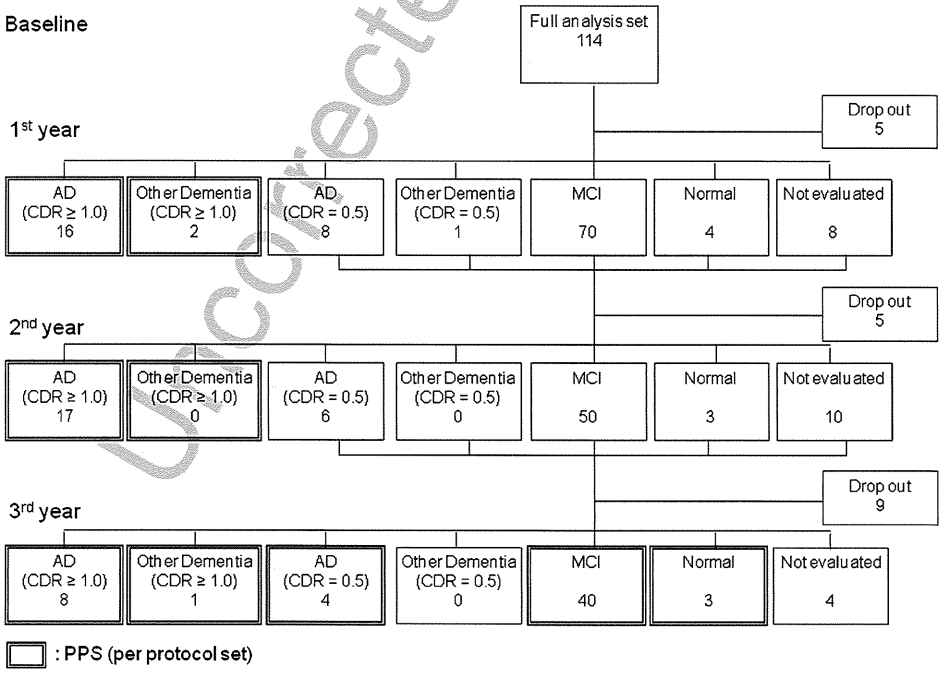

Fig. 1. Schematic summary of clinical outcomes in all MCI cases. Originally, 114 patients with MCI were included. A total of 23 patients dropped out during the 3 years. Our final sample size for the analyses of PET images was 88 patients (excluding 3 patients who converted to other dementias).

Table 1
Demographic and neuropsychological data at baseline

	AD converter (n=41) Mean (SD)	Non-converter (n=47) Mean (SD)
Age	71.2 (6.5)	70.5 (6.7)
Education (year)	12.1 (3.2)	11.8 (3.0)
WMS-R-LMI**	6.3 (3.3)	9.4 (3.2)
WMS-R-LMII**	1.7 (2.2)	4.1 (2.9)
MMSE*	25.6 (1.7)	26.9 (2.0)
ADAS*	10.6 (5.0)	7.6 (4.3)
GDS*	4.9 (2.2)	3.4 (2.0)

WMS-R-LM, Wechsler Memory Scale–Revised Logical Memory; MMSE, Mini-Mental State Examination; ADAS, Alzheimer's Disease Assessment Scale; GDS, Geriatric Depression Scale.

PET image interpretation

As the result of image interpretation, P1 and P1+ patterns were observed in 69.9% and 8.0%, respectively, and the other patterns were observed in 22.1%, including the P2 pattern in 4.4%, of all the amnestic MCI patients (Fig. 2). In this study, all P1+ cases showed a P1 pattern with occipital hypometabolism. Therefore, we combined the P1 pattern and P1+ pattern as an AD/DLB pattern for calculating the diagnostic performance.

Silverman's classification in the central image interpretation completely matched in 53% of cases, and two or more complete matches from three raters were achieved in 91% of cases. Since the P1 pattern accounted for about 70% of cases in the image interpretation, the frequency distribution of the Silverman's classification was significantly biased. A significant deviation in the distribution increases the probability of accidental match, making it difficult to correctly evaluate the degree of agreement.

The image interpretation based on the classification of PET images predicted conversion to AD during 3-year follow-up with an overall diagnostic accuracy of 68%, a sensitivity of 98%, and a specificity of 41% for the full analysis data set of the 88 subjects in this study.

The diagnostic parameters for each follow-up interval are summarized in Table 2.

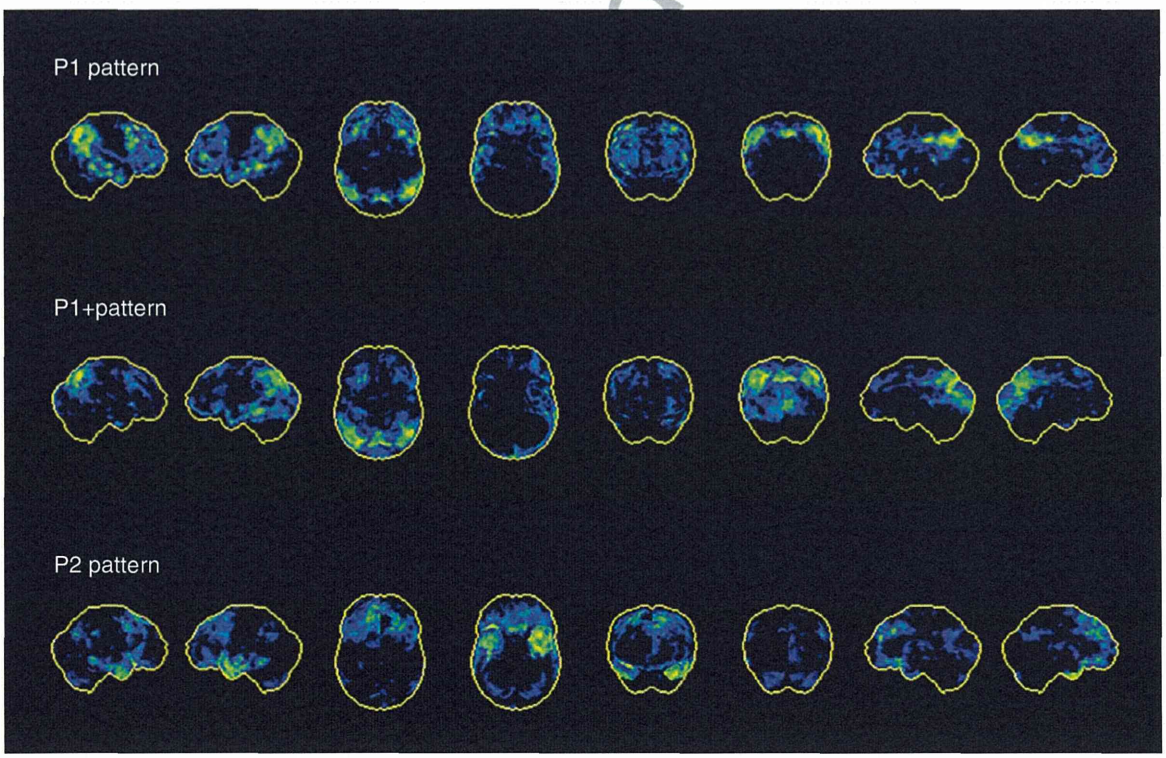

Fig. 2. 3D-SSP z-score maps showing hypometabolism in the progressive pattern groups (P1 pattern group, P1+ pattern group, and P2 pattern group) in comparison with the normal database are shown. From left to right, 3D-SSP maps are shown on the right lateral, left lateral, superior, inferior, anterior, posterior, and right and left middle views of a standardized brain image.

Table 2
Diagnostic parameters

Variable	Follow-up intervals (y)	AUC (95% CI)	Cutoff	SEN	SPE	ACC	PPV	NPV
PET visual interpretation	1	–	–	1.00	0.22	0.35	0.21	1.00
	2	–	–	0.97	0.32	0.56	0.45	0.95
	3	–	–	0.98	0.41	0.68	0.60	0.95
PET score	1	0.708 (0.569–0.846)	1.03	0.69	0.75	0.74	0.34	0.93
	2	0.809 (0.714–0.905)	1.03	0.70	0.90	0.83	0.79	0.84
	3	0.747 (0.641–0.852)	1.03	0.61	0.91	0.77	0.86	0.73
VSRAD z-score	1	0.679 (0.533–0.825)	1.47	0.75	0.57	0.60	0.26	0.92
	2	0.684 (0.570–0.799)	1.44	0.69	0.64	0.66	0.51	0.79
	3	0.658 (0.543–0.774)	1.44	0.64	0.64	0.64	0.60	0.68

AUC, area under the curve; SEN, sensitivity; SPE, specificity; ACC, accuracy; PPV, positive predictive value; NPV, negative predictive value.

PET score

The PET scores at baseline were 1.26 ± 0.69 for the AD converters and 0.70 ± 0.44 for the non-converters, respectively ($p < 0.001$). It was hypothesized that subjects who had a PET score at baseline above 1.0 had a significantly increased risk for progression. The statistics for predicting progression during 3-year follow-up were sensitivity, 61%; specificity, 79%; and accuracy, 70%. When mean PET scores were calculated according to conversion time, converters in the 1st and 2nd year showed a significantly higher PET score compared to that of non-converters. In contrast, converters in the 3rd year showed no difference in the mean PET score compared to non-converters (Fig. 3). The diagnostic accuracy during the 2-year follow-up was more promising, with an overall diagnostic accuracy of 76%, a sensitivity of 70%, and a specificity of 80%.

Area under the curve of ROC analysis for the PET score was greatest for 2-year follow-up. The ROC-derived PET score thresholds obtained using Youden index [28] yielded an adjusted accuracy of 83%, with 70% sensitivity and 90% specificity at a threshold value of PET score = 1.03 during 2-year follow-up. The diagnostic parameters for each follow-up interval are summarized in Table 2.

MRI

Because four cases at one institution were examined exceptionally with a 3T MRI system, those four were excluded from further analysis.

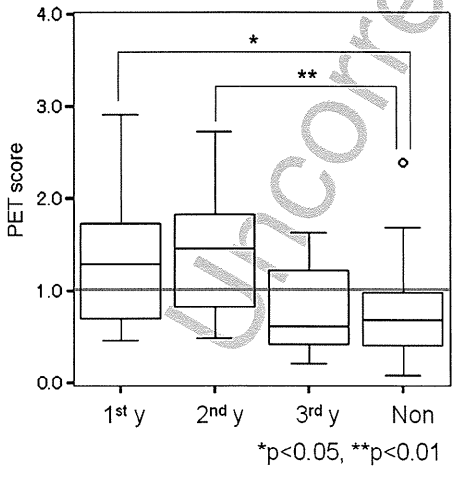

Fig. 3. Box plot of baseline PET scores (interquartile and full range) for converters according to conversion time. MCI patients progressing to AD in the 1st and 2nd year have significantly higher scores than non-converters ($p < 0.05$ and $p < 0.01$ in Tukey multiple comparisons). 1st y = 1st year converter, 2nd y = 2nd year converter, 3rd y = 3rd year converter, and Non = non-converter.

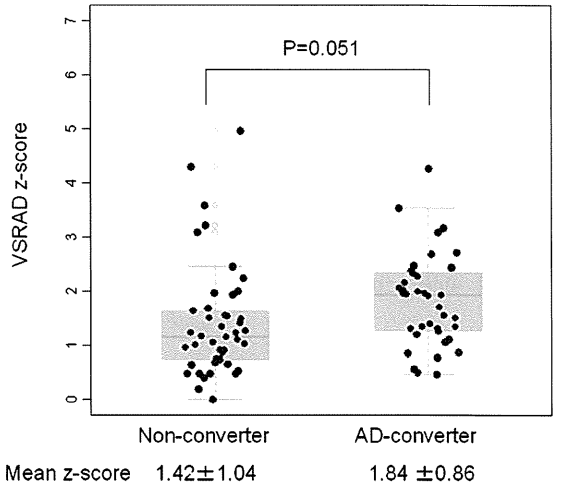

Fig. 4. Comparison between AD converters and non-converters on VSRAD z-scores in the target VOI for the left medial temporal structures. There was no significant difference between the two groups ($p = 0.051$). VSRAD, voxel-based specific regional analysis system for Alzheimer's disease.

For the AD converters and non-converters, the bilateral mean z-scores in the target VOI for the medial temporal structures at baseline were 1.84 ± 0.75 and 1.57 ± 1.01, respectively ($p = 0.191$); the right side mean z-scores were 1.80 ± 0.93 and 1.66 ± 1.13, respectively ($p = 0.543$); and the left side mean z-scores were 1.84 ± 0.86 and 1.42 ± 1.04, respectively ($p = 0.051$). Thus, the AD converters showed a tendency toward higher mean z-score in the target VOI for the left medial temporal structures but did not reach significance (Fig. 4).

Area under the curve of ROC analysis for VSRAD z-score was greatest for 2-year follow-up (Table 2). The ROC-derived thresholds using Youden index [28] for VSRAD mean z-score yielded an adjusted accuracy of 66%, with 69% sensitivity, and 64% specificity at a threshold value of VSRAD z-score = 1.44 during 2-year follow-up.

Logistic regression analysis

Multivariate logistic regression analysis identified PET score and WMS-R-LM II as predictors distinguishing AD converters from non-converters over 2 years. When age, gender, education level, WMS-R-LM II, and PET score were submitted to the forced entry procedure, AD conversion was associated significantly with the PET score ($p < 0.0001$; odds ratio, 28.25; 95% confidence interval [CI], 6.02–132.6) and WMS-R-LM II ($p = 0.001$; odds ratio, 0.61; 95% CI, 0.46–0.81) (Table 3). The combination of PET score and WMS-R-LM II distinguished AD converters from non-converters with 84.8% accuracy, 72.7% sensitivity, and 91.5% specificity.

DISCUSSION

In this study, 41 (47%) of 88 MCI patients progressed to AD. The annual conversion rate was 15.7% during the 3-year follow-up. These results are consistent with reports from other groups, indicating that, annually, 12% to 15% of amnestic MCI patients progress to AD [1].

Group comparisons based on classification of the PET image interpretations demonstrated heterogeneity in ^{18}F-FDG-PET among subjects with amnestic MCI (Fig. 2). Although the progressive pattern included the P1 pattern (69.9%), the P1+ pattern (8.0%), and the P2 pattern (4.4%), 41 (93.2%) of 44 converters were AD converters with 3 converting to DLB, FTD, and VaD.

The frequency of the P1+ pattern in the absence of DLB was relatively high. We reported that 28% of patients with AD had reduced blood flow in the occipital lobe [29]. Additionally, in our prospective SPECT study to examine the value of ^{123}I-N-Isopropyl-4-Iodoamphetamine cerebral blood flow SPECT with regard to early diagnosis of AD in patients with MCI, the frequency of the DLB pattern was 18.7% of all patients with amnestic MCI [30]. We assumed that older patients in general tend to have reduced blood flow or glucose metabolism in the occipital lobe, including those with AD. This is a topic for a future study.

Because we considered that differentiating between AD and DLB based on reduced blood flow or glucose metabolism in the occipital lobe was difficult and that PET scores do not distinguish DLB from AD, we applied pooling of the P1 pattern with the P1+ pattern in this study in the same way as in our previous SPECT study [30]. Although we analyzed the data for the P1 pattern only, the results were almost the same as those when pooling P1 with P1+(data not shown). Therefore, we believe that combining the P1 pattern with the P1+ pattern as an AD/DLB pattern to investigate the role of ^{18}F-FDG-PET in predicting conversion to AD is not problematic. The clinical significance of the heterogeneity in ^{18}F-FDG-PET should be further evaluated.

The diagnostic performance of ^{18}F-FDG-PET was calculated based on the clinical outcomes after 3 years of follow-up. The PET image interpretation showed a high sensitivity for detection of AD-converters, but its specificity was relatively low. Low specificity

Table 3
Results of multivariate logistic regression analyses for predictors of AD conversion

Variable	Coefficient (B)	SE	Wald	df	*p* value	Odds ratios	95% CI	
Age	0.019	0.063	0.092	1	0.761	1.019	0.901	1.153
Gender	−0.958	0.743	1.662	1	0.197	0.384	0.089	1.646
Education level	0.041	0.114	0.129	1	0.720	1.042	0.833	1.303
WMS-R-LMII	−0.502	0.146	11.887	1	0.001	0.605	0.455	0.805
PET score	3.341	0.789	17.942	1	<0.0001	28.252	6.021	132.572
Constant	−4.051	4.994	0.658	1	0.417	0.017		

df, degree of freedom; CI, confidence Interval; WMS-R-LM, Wechsler Memory Scale–Revised Logical Memory.

indicated that some non-converters showed AD/DLB-like hypometabolism on ^{18}F-FDG-PET images. These results were not in line with previous reports [7–11] where higher specificity and diagnostic accuracy were reported. The true reason for low specificity in spite of a longer follow-up compared to previous reports is unclear. One possible explanation is the difference in the characteristics of registered MCI patients for each study. In fact, conversion rates from MCI to AD were very high in some studies. Such an increase in the ratio of converters may result in a decrease in false-positive cases.

Considering the higher mean PET scores of converters in the 1st and 2nd year of follow-up, we hypothesized that the rapid converters showed more distinct AD/DLB-like hypometabolism compared to the slower converters. Although a threshold effect might exist, overall accuracy of the PET score was better than that of visual assessment at all time intervals, as shown in Table 2. As the PET score is a numerical index, PET score threshold can be optimized to maximize the prediction accuracy. The best performance of PET score was achieved at the 2-year follow-up interval. In other words, the PET score was efficient at identifying rapid converters during the 2-year follow-up.

Multivariate logistic regression analysis demonstrated that the PET score derived from ^{18}F-FDG-PET was the most significant predictor for conversion to AD among amnestic MCI patients across institutions where various types of PET or PET-CT devices were used. These results were in line with recent reports using data from the Alzheimer's Disease Neuroimaging Initiative [12–14]. Furthermore, WMS-R-LM was identified as a significant predictor for conversion to AD. A combination of statistically significant predictors, both PET score and WMS-R-LM, could assist in early stratification of patients into high- or low-risk groups.

On the other hand, the VSRAD® z-score for MRI failed to identify MRI as a predictor to distinguish AD converters from non-converters. Our results were in line with a previous study showing that ^{18}F-FDG PET is a better predictor of conversion than MR imaging [12, 14]. The possible reasons why FDG PET offers greater accuracy or sensitivity than other biomarkers at the MCI stage are not fully understood, although there is growing consensus that metabolic deficits are greater in magnitude than volumetric changes earlier in the disease.

The present study had some limitations. First, our neuropsychological test batteries were limited and did not include tests specifically designed to assess cognitive function for the early diagnosis of AD, although the MMSE and WMS-R-LM are more practical for use in a routine clinical scenario. Second, the mean age of individuals in the normal database for 3D-SSP was lesser than that of the patient group. Further analysis would be needed using an age-matched normal database. Third, although only a VBM using VSRAD® was used to evaluate volumetric changes of MRI, different methodologies such as cortical approaches rather than voxel-based approaches should be further applied [31]. Fourth, the primary outcome (conversion to AD) contained some error because some patients classified as non-converters may convert to AD with longer follow-up. Therefore, improvement of specificity and diagnostic accuracy of the PET image interpretation can be expected due to a decrease in false-positive cases provided by a longer follow-up period.

CONCLUSIONS

Visually assessed ^{18}F-FDG-PET is a very sensitive but relatively nonspecific measure for predicting conversion to AD in patients with MCI. On the other hand, the PET score is the most statistically significant predictive factor for conversion from MCI to AD, and the diagnostic performance of the PET score is more promising for rapid converters over 2 years.

ACKNOWLEDGMENTS

The authors are indebted to Professor Daniel Hillel Silverman for his valuable and constructive suggestions regarding this paper.

This work was supported by the Health Labour Sciences Research Grant from the Ministry of Health, Labour, and Welfare of Japan (H17-Tyojyu-023) and the Research Funding for Longevity Sciences from National Center for Geriatrics and Gerontology, Japan (20-1). The authors thank those people who contributed to the subjects' care and to the collection of PET images and clinical reports.

This study is registered UMIN ID: C000000297.

The funding sources had no role in study design, data collection, data analyses, or data interpretation.

Authors' disclosures available online (http://j-alz.com/manuscript-disclosures/14-1338r1).

SUPPLEMENTARY MATERIAL

The supplementary material is available in the electronic version of this article: http://dx.doi.org/10.3233/JAD-141338.

REFERENCES

[1] Petersen RC (2004) Mild cognitive impairment as a diagnostic entity. *J Intern Med* **256**, 183-194.

[2] Dubois B, Feldman HH, Jacova C, Dekosky ST, Barberger-Gateau P, Cummings J, Delacourte A, Galasko D, Gauthier S, Jicha G, Meguro K, O'brien J, Pasquier F, Robert P, Rossor M, Salloway S, Stern Y, Visser PJ, Scheltens P (2007) Research criteria for the diagnosis of Alzheimer's disease: Revising the NINCDS-ADRDA criteria. *Lancet Neurol* **6**, 734-746.

[3] Dubois B, Feldman HH, Jacova C, Cummings JL, Dekosky ST, Barberger-Gateau P, Delacourte A, Frisoni G, Fox NC, Galasko D, Gauthier S, Hampel H, Jicha GA, Meguro K, O'Brien J, Pasquier F, Robert P, Rossor M, Salloway S, Sarazin M, de Souza LC, Stern Y, Visser PJ, Scheltens P (2010) Revising the definition of Alzheimer's disease: A new lexicon. *Lancet Neurol* **9**, 1118-1127.

[4] Albert MS, DeKosky ST, Dickson D, Dubois B, Feldman HH, Fox NC, Gamst A, Holtzman DM, Jagust WJ, Petersen RC, Snyder PJ, Carrillo MC, Thies B, Phelps CH (2011) The diagnosis of mild cognitive impairment due to Alzheimer's disease: Recommendations from the National Institute on Aging-Alzheimer's Association workgroups on diagnostic guidelines for Alzheimer's disease. *Alzheimers Dement* **7**, 270-279.

[5] Sperling RA, Aisen PS, Beckett LA, Bennett DA, Craft S, Fagan AM, Iwatsubo T, Jack CR Jr, Kaye J, Montine TJ, Park DC, Reiman EM, Rowe CC, Siemers E, Stern Y, Yaffe K, Carrillo MC, Thies B, Morrison-Bogorad M, Wagster MV, Phelps CH (2011) Toward defining the preclinical stages of Alzheimer's disease: Recommendations from the National Institute on Aging-Alzheimer's Association workgroups on diagnostic guidelines for Alzheimer's disease. *Alzheimers Dement* **7**, 280-292.

[6] McKhann GM, Knopman DS, Chertkow H, Hyman BT, Jack CR Jr, Kawas CH, Klunk WE, Koroshetz WJ, Manly JJ, Mayeux R, Mohs RC, Morris JC, Rossor MN, Scheltens P, Carrillo MC, Thies B, Weintraub S, Phelps CH (2011) The diagnosis of dementia due to Alzheimer's disease: Recommendations from the National Institute on Aging-Alzheimer's Association workgroups on diagnostic guidelines for Alzheimer's disease. *Alzheimers Dement* **7**, 263-269.

[7] Anchisi D, Borroni B, Franceschi M, Kerrouche N, Kalbe E, Beuthien-Beumann B, Cappa S, Lenz O, Ludecke S, Marcone A, Mielke R, Ortelli P, Padovani A, Pelati O, Pupi A, Scarpini E, Weisenbach S, Herholz K, Salmon E, Holthoff V, Sorbi S, Fazio F, Perani D (2005) Heterogeneity of brain glucose metabolism in mild cognitive impairment and clinical progression to Alzheimer disease. *Arch Neurol* **62**, 1728-1733.

[8] Arnaiz E, Jelic V, Almkvist O, Wahlund LO, Winblad B, Valind S, Nordberg A (2001) Impaired cerebral glucose metabolism and cognitive functioning predict deterioration in mild cognitive impairment. *Neuroreport* **12**, 851-855.

[9] Mosconi L, Perani D, Sorbi S, Herholz K, Nacmias B, Holthoff V, Salmon E, Baron JC, De Cristofaro MT, Padovani A, Borroni B, Franceschi M, Bracco L, Pupi A (2004) MCI conversion to dementia and the APOE genotype: A prediction study with FDG-PET. *Neurology* **63**, 2332-2340.

[10] Drzezga A, Grimmer T, Riemenschneider M, Lautenschlager N, Siebner H, Alexopoulus P, Minoshima S, Schwaiger M, Kurz A (2005) Prediction of individual clinical outcome in MCI by means of genetic assessment and (18)F-FDG PET. *J Nucl Med* **46**, 1625-1632.

[11] Silverman DHS, Truong CT, Kim SK, Chang CY, Chen W, Kowell AP, Cummings JL, Czernin J, Small GW, Phelps ME (2003) Prognostic value of regional cerebral metabolism in patients undergoing dementia evaluation: Comparison to a quantifying parameter of subsequent cognitive performance and to prognostic assessment without PET. *Mol Genet Metab* **80**, 350-355.

[12] Landau SM, Harvey D, Madison CM, Reiman EM, Foster NL, Aisen PS, Petersen RC, Shaw LM, Trojanowski JQ, Jack CR Jr, Weiner MW, Jagust WJ (2010) Alzheimer's Disease Neuroimaging Initiative. Comparing predictors of conversion and decline in mild cognitive impairment. *Neurology* **75**, 230-238.

[13] Chen K, Ayutyanont N, Langbaum JBS, Fleisher AS, Reschke C, Lee W, Liu X, Bandy D, Alexander GE, Thompson PM, Shaw L, Trojanowski JQ, Jack CR Jr, Landau SM, Foster NL, Harvey DJ, Weiner MW, Koeppe RA, Jagust WJ, Reiman EM (2011) Alzheimer's Disease Neuroimaging Initiative. Characterizing Alzheimer's disease using a hypometabolic convergence index. *Neuroimage* **56**, 52-60.

[14] Shaffer JL, Petrella JR, Sheldon FC, Choudhury KR, Calhoun VD, Coleman RE, Doraiswamy PM (2013) Alzheimer's Disease Neuroimaging Initiative. Predicting cognitive decline in subjects at risk for Alzheimer disease by using combined cerebrospinal fluid, MR imaging, and PET biomarkers. *Radiology* **266**, 583-591.

[15] Silverman DH, Small GW, Chang CY, Lu CS, Kung De Aburto MA, Chen W, Czernin J, Rapoport SI, Pietrini P, Alexander GE, Schapiro MB, Jagust WJ, Hoffman JM, Welsh-Bohmer KA, Alavi A, Clark CM, Salmon E, de Leon MJ, Mielke R, Cummings JL, Kowell AP, Gambhir SS, Hoh CK, Phelps ME (2001) Positron emission tomography in evaluation of dementia: Regional brain metabolism and long-term outcome. *JAMA* **286**, 2120-2127.

[16] Herholz K, Salmon E, Perani D, Baron JC, Holthoff V, Frölich L, Schönknecht P, Ito K, Mielke R, Kalbe E, Zündorf G, Delbeuck X, Pelati O, Anchisi D, Fazio F, Kerrouche N, Desgranges B, Eustache F, Beuthien-Baumann B, Menzel C, Schröder J, Kato T, Arahata Y, Henze M, Heiss WD (2002) Discrimination between Alzheimer dementia and controls by automated analysis of multicenter FDG PET. *Neuroimage* **17**, 302-316.

[17] Haense C, Herholz K, Jagust WJ, Heiss WD (2009) Performance of FDG PET for detection of Alzheimer's disease in two independent multicenter samples (NEST-DD and ADNI). *Dement Geriatr Cogn Disord* **28**, 259-266.

[18] Herholz K, Westwood S, Haense C, Dunn G (2011) Evaluation of a calibrated (18)F-FDG PET score as a biomarker for progression in Alzheimer disease and mild cognitive impairment. *J Nucl Med* **52**, 1218-1226.

[19] Hirata Y, Matsuda H, Nemoto K, Ohnishi T, Hirao K, Yamashita F, Asada T, Iwabuchi S, Samejima H (2005) Voxel-based morphometry to discriminate early Alzheimer's disease from controls. *Neurosci Lett* **382**, 269-274.

[20] Matsuda H (2007) Role of neuroimaging in Alzheimer's disease, with emphasis on brain perfusion SPECT. *J Nucl Med* **48**, 1289-1300.

[21] Matsuda 21, H (2007) The role of neuroimaging in mild cognitive impairment. *Neuropathology* **27**, 570-577.

[22] Niida R, Niida A, Motomura M, Uechi A (2011) Diagnosis of depression by MRI scans with the use of VSRAD-a promising auxiliary means of diagnosis: A report of 10 years research. *Int J Gen Med* **4**, 377-387.

[23] Matsuda H, Mizumura S, Nemoto K, Yamashita F, Imabayashi E, Sato N, Asada T (2012) Automatic voxel-based morphometry of structural MRI by SPM8 plus diffeomorphic anatomic

registration through exponentiated lie algebra improves the diagnosis of probable Alzheimer disease. *AJNR Am J Neuroradiol* **33**, 1109-1114.

[24] Roman GC, Tatemichi TK, Erkinjuntti T, Cummings JL, Masdeu JC, Garcia JH, Amaducci L, Orgogozo JM, Brun A, Hofman A, Moody DM, O'Brien MD, Yamaguchi T, Grafman J, Drayer BP, Bennett DA, Fisher M, Ogata J, Kokmen E, Bermejo F, Wolf PA, Gorelick PB, Bick KL, Pajeau AK, Bell MA, DeCarli C, Culebras A, Korczyn AD, Bogousslavsky J, Hartmann A, Scheinberg P (1993) Vascular dementia: Diagnostic criteria for research studies-report of the NINDS-AIRENS International Workshop. *Neurology* **43**, 250-260.

[25] McKeith IG, Galasko D, Kosaka K, Perry EK, Dickson DW, Hansen LA, Salmon DP, Lowe J, Mirra SS, Byrne EJ, Lennox G, Quinn NP, Edwardson JA, Ince PG, Bergeron C, Burns A, Miller BL, Lovestone S, Collerton D, Jansen EN, Ballard C, de Vos RA, Wilcock GK, Jellinger KA, Perry RH (1996) Consensus guidelines for the clinical and pathologic diagnosis of dementia with Lewy bodies (DLB): Report of the Consortium on DLB International Workshop. *Neurology* **47**, 1113-1124.

[26] McKhann G, Albert MS, Grossman M, Miller B, Dickson D, Trojanowski JQ (2001) Clinical and pathological diagnosis of frontotemporal dementia. *Ann Neurol* **58**, 1803-1809.

[27] Knopman DS, DeKosky ST, Cummings JL, Chui H, Corey-Bloom J, Relkin N, Small GW, Miller B, Stevens JC (2001) Practice parameter: Diagnosis of dementia (an evidence-based review). Report of the Quality Standards Subcommittee of the American Academy of Neurology. *Neurology* **56**, 1143-1153.

[28] Youden WJ (1950) Index for rating diagnostic tests. *Cancer* **3**, 32-35.

[29] Ishii K, Ito K, Nakanishi A, Kitamura S, Terashima A (2014) Computer-assisted system for diagnosing degenerative dementia using cerebral blood flow SPECT and 3D-SSP: A multicenter study. *Jpn J Radiol* **32**, 383-390.

[30] Ito K, Mori E, Fukuyama H, Ishii K, Washimi Y, Asada T, Mori S, Meguro K, Kitamura S, Hanyu H, Nakano S, Matsuda H, Kuwabara Y, Hashikawa K, Momose T, Uchida Y, Hatazawa J, Minoshima S, Kosaka K, Yamada T, Yonekura Y, Study J-COSMIC, Group (2013) Prediction of outcomes in MCI with (123)I-IMP-CBF SPECT: A multicenter prospective cohort study. *Ann Nucl Med* **27**, 898-906.

[31] Cuingnet R, Gerardin E, Tessieras J, Auzias G, Lehericy S, Habert MO, Chupin M, Benali H, Colliot O (2010) Alzheimer's Disease Neuroimaging Initiative. Automatic classification of patients with Alzheimer's disease from structural MRI: A comparison of ten methods using the ADNI database. *Neuroimage* **56**, 766-781.

Jpn J Radiol (2014) 32:383–390
DOI 10.1007/s11604-014-0329-6

ORIGINAL ARTICLE

Computer-assisted system for diagnosing degenerative dementia using cerebral blood flow SPECT and 3D-SSP: a multicenter study

Kazunari Ishii · Kengo Ito · Atsushi Nakanishi · Shin Kitamura · Akira Terashima

Received: 10 January 2014 / Accepted: 16 April 2014 / Published online: 17 May 2014

Abstract
Purpose Due to increasing numbers of patients with dementia, more physicians who do not specialize in brain nuclear medicine are being asked to interpret SPECT images of cerebral blood flow. We conducted a multicenter study to determine whether a computer-assisted diagnostic system *Z*-score summation analysis method (ZSAM) using three-dimensional stereotactic surface projections (3D-SSP) can differentiate Alzheimer's disease (AD)/dementia with Lewy bodies (DLB) and non-AD/DLB in institutions using various types of gamma cameras.
Method We determined the normal thresholds of *Z*-sum (summed *Z*-score) within a template region of interest for each single photon emission computed tomography (SPECT) device and then compared them with the *Z*-sums of patients and calculated the accuracy of the differential diagnosis by ZSAM. We compared the diagnostic accuracy between ZSAM and visual assessment.
Patients We enrolled 202 patients with AD (mean age, 76.8 years), 40 with DLB (mean age 76.3 years) and 36 with non-AD/DLB (progressive supranuclear palsy, $n = 10$; frontotemporal dementia, $n = 20$; slowly progressive aphasia, $n = 2$ and one each with idiopathic normal pressure hydrocephalus, corticobasal degeneration, multiple system atrophy and Parkinson's disease) who underwent *N*-isopropyl-*p*-[^{123}I] iodoamphetamine cerebral blood flow SPECT imaging at each participating institution.
Results The ZSAM sensitivity to differentiate between AD/DLB and non-AD/DLB in all patients, as well as those with mini-mental state examination scores of ≥24 and 20–23 points were 88.0, 78.0 and 88.4 %, respectively, with specificity of 50.0, 44.4 and 60.0 %, respectively. The diagnostic accuracy rates were 83.1, 72.9 and 84.2 %, respectively. The areas under receiver operating characteristics curves for visual inspection by four expert raters were 0.74–0.84, 0.66–0.85 and 0.81–0.93, respectively, in the same patient groups. The diagnostic accuracy rates were 70.9–89.2 %, 50.9–84.8 % and 76.2–93.1 %, respectively.
Conclusion The diagnostic accuracy of ZSAM to differentiate AD/DLB from other types of dementia or degenerative diseases regardless of severity was equal to that of visual assessment by expert raters even across several institutions. These findings suggested that ZSAM could serve as a supplementary tool to help expert evaluators who differentially diagnose dementia from SPECT images by visual assessment.

Keywords Alzheimer's disease · Lewy bodies · Cerebral blood flow · *Z*-score summation analysis · Dementia

K. Ishii (✉)
Department of Radiology, Faculty of Medicine, Kinki University, 377-2 Osakasayama, Osaka 589-8511, Japan
e-mail: kishii@hbhc.jp; ishii@med.kindai.ac.jp

K. Ito
Department of Clinical and Experimental Neuroimaging, Center for Development of Advanced Medicine for Dementia, National Center for Geriatrics and Gerontology, Obu, Aichi, Japan

A. Nakanishi
Department of Radiology, School of Medicine, Juntendo University, Tokyo, Japan

S. Kitamura
Department of Internal Medicine, Nippon Medical School Musashi Kosugi Hospital, Kawasaki, Kanagawa, Japan

A. Terashima
Institute for Aging Brain and Cognitive Disorders, Hyogo Brain and Heart Center, Himeji, Hyogo, Japan

Introduction

Society is rapidly aging, and the increase in the numbers of patients with dementia is posing considerable medical and social problems. Alzheimer's disease (AD) is the most common degenerative dementia, and it can be diagnosed by functional brain imaging using fluorodeoxyglucose (FDG) positron emission tomography (PET) and SPECT [1, 2]. Although PET can diagnostically differentiate AD more precisely than SPECT, PET costs are not covered by insurance in many European countries and in Japan. Thus, FDG-PET is not used in the medical care of patients with dementia, and cerebral blood flow SPECT is exclusively used because it is covered by insurance. As the number of patients with dementia has increased, physicians who are not specialists in cerebral nuclear medicine are often obliged to interpret cerebral blood flow SPECT images. Atypical findings are obvious on cerebral blood flow SPECT images of dementia, but subtle differences can be difficult even for experts in brain nuclear medicine to diagnose. On the other hand, a statistical image analysis provides a tangible result, since it is determined based on specific criteria. A computer-assisted diagnostic system has shown promise as a supplementary measure for interpreting cerebral blood flow SPECT images [3]. We conducted a multicenter study to determine its applicability.

Patients and methods

Procedure

The analysis *Z*-score summation analysis method (ZSAM) using the computer-assisted diagnostic system as described [3] comprises the following procedures.

1. The IMP-SPECT images of normal individuals are analyzed using 3D-SSP [4] to generate *Z*-score images. *Z*-scores are calculated using the following formula: *Z*-score = ([normal mean] − [individual value])/(normal standard deviation). Summed positive *Z*-scores (*Z*-sum) are obtained from template ROIs (parietal lobe, posterior cingulate gyrus and precuneus, medial surface of the occipital lobe and the lateral surface of the occipital lobe) that are regions of characteristic blood flow reduction in *Z*-score images of AD and DLB. This is because each ROI includes negative and positive *Z*-scores and reduced blood flow appears as a positive *Z*-score.
2. The *Z*-sum of some normal individuals is averaged for each ROI and the normal threshold of the *Z*-sum with the mean value and standard deviation is calculated.
3. The *Z*-sum of patients processed by the same procedure as (1) is compared with the normal threshold calculated above in (2).
4. Blood flow is considered to be reduced if the *Z*-sum of the patient exceeds the normal threshold.

Various SPECT devices are used for cerebral blood flow SPECT, and a normal database that conforms to each SPECT device is used in 3D-SSP analysis. This multicenter study determines whether AD/DLB can be differentiated from other types of dementia and degenerative diseases using new template ROIs and the normal thresholds of the *Z*-sum set for each normal database.

Patients

The study proceeded according to the clinical study guidelines of each institution and was approved by each independent ethics committee.

Preparation of template ROIs (group 1)

We prepared template ROIs from 36 patients with probable AD and 13 with probable dementia with Lewy bodies (DLB) who underwent cerebral blood flow SPECT with IMP using a Siemens e.cam at the Hyogo Brain and Heart Center between August and December in 2008. We used the diagnostic criteria of the Neurological and Communicative Disorders and Stroke-Alzheimer's Disease and Related Disorders Association (NINCDS/ADRDA) for AD [5] and those of the third report of the Dementia with Lewy Bodies Consortium for DLB [6]. Patients with cerebrovascular disease were excluded in this study. A normal database created from 29 normal volunteers specifically prepared for the Siemens e.cam by Onishi et al. [7] served as the comparative group. The patients in the AD, DLB and normal database groups were 78.1 ± 6.4, 75.9 ± 6.6, and 64.2 ± 8.2 years old, respectively, and the MMSE scores of the AD and DLB groups were 20.7 ± 3.8 and 19.4 ± 7.4 points, respectively.

Diagnostic performance review (group 2)

The diagnostic performance of ZSAM was determined based on data from 202 patients diagnosed with probable AD according to the NINCDS-ADRDA diagnostic criteria [5], 40 diagnosed with probable DLB based on the third report of the DLB Consortium diagnostic criteria [6], 20 with FTD who met FTD diagnostic criteria [8], 10 with PSP who met the National Institute of Neurological Disorders and the Society for Progressive Supranuclear Palsy (NINDS-SPSP) International Workshop diagnostic criteria [9], two with slowly-progressive

aphasia, and one each with iNPH, CBD, MSA and PD who presented at the medical institutions involved in this study between December 2007 and February 2011. The slowly progressive aphasia (SPA), iNPH, CBD, MSA, and PD were diagnosed according to disease-specific criteria [10–13]. The mean ± SD of age (years) and MMSE scores for AD, DLB, FTD, PSP and SPA were 76.8 ± 7.2 and 19.4 ± 4.7, 76.3 ± 5.7 and 20.2 ± 5.0, 70.6 ± 9.0 and 20.1 ± 5.5, 71.6 ± 6.6 and 21.6 ± 4.6, and 64.5 ± 1.5 and 21.0 ± 1.0, respectively. The age (years) and MMSE scores for those with iNPH, CBD, MSA and PD were 76 and 17, 64 and 23, 82 and 22, and 83 and 23, respectively. Both AD and DLB were included in the AD/DLB group, and FTD, PSP, SPA, iNPH, CBD, MSA, and PD were included in the non-AD/DLB group. We selected patients with MMSE scores of ≥24 and 20–23 points to determine the diagnostic accuracy of ZSAM for mild disease (Table 1).

Table 1 Demographic data of the subjects

Group	Number	Age (years)	MMSE (score)
First Group			
AD	36	78.1±6.4	20.7±3.8
DLB	13	75.9±6.6	19.4±7.4
Second Group all			
AD/DLB_group			
AD	202	76.8±7.2	19.4±4.7
DLB	40	76.3±5.7	20.2±5.0
nonAD/nonDLB_group	36	71.1±8.4	20.7±4.9
Second Group MMSE 24 and more			
AD/DLB_group			
AD	40	75.3±6.3	25.4±1.6
DLB	10	73.0±6.8	25.6±1.3
nonAD/nonDLB_group	9	69.3±6.6	26.0±1.5
Second Group MMSE 20-23			
AD/DLB_group			
AD	72	77.2±6.6	21.3±1.1
DLB	14	77.1±4.5	22.1±1.0
nonAD/nonDLB_group	15	72.6±9.2	22.1±0.9

SPECT image acquisition and processing

Imaging was started in the resting state 15 min after an injection of 111–222 MBq (3–6 mCi) of IMP. Table 2 lists the SPECT equipment and reconstruction conditions.

Creation of new template ROI maps

We performed stereotactic anatomic standardization as follows. The original IMP-SPECT image data were transformed into standard Talairach space using the NEUROSTAT program [4], which is the basis of 3D-SSP (Satoshi Minoshima, Department of Radiology and Bioengineering, University of Washington, Seattle, WA, USA). Detailed procedure of 3D-SSP and this program is described in the previous literature [3]. In this study, we used pixel values of individual surface maps normalized to values for mean activity in the whole brain. As a new AD/DLB template ROI map, pixels with significantly decreased perfusion in the AD group ($p < 0.05$), obtained from a comparison between the SIEMENS e.cam normal database and the AD group (first group) were plotted (Fig. 1), and as an occipital template ROI map, pixels with significantly decreased perfusion in the DLB group ($p < 0.05$), obtained from a comparison between the AD and DLB groups (first group) were plotted (Fig. 1). To create an ROI template with significantly decreased symmetrical areas in this map, larger areas than the opposite sides were set to make both sides the same size, which increased detection sensitivity in a brain with AD.

Threshold values of summed positive Z-scores

We calculated the threshold Z-sum in the new template ROI maps for diagnosis using the following jackknife-type technique. First, one patient from the normal group was selected to constitute a normal database and another normal database was prepared from the remainder of the normal group. The normal database constructed based on data from the selected normal patient was analyzed with 3D-SSP to prepare a Z-score image. The procedure was repeated for each patient in the normal database. The AD/DLB and occipital template ROI were set in the Z-score images of

Table 2 Characteristics of the SPECT study and normal database (NDB) at each institute

Institution	Camera type	Prefilter	Collimator	Cutoff frequency	Scatter correction	Attenuation correction	Matrix size	Pixel size (mm)
A	TOSHIBA GCA9300	Butterworth	LESHR-Fanbeam	0.08 cycles/pixel	TEW	Chang	128 × 128	1.72
B	TOSHIBA ECAM	Butterworth	LMEGP	0.45 cycles/pixel	non	Chang	128 × 128	3.9
C	SIEMENS e.cam	Butterworth	LMEGP	0.40 Nyquist	MEW	Chang	128 × 128	3.9
D	SIEMENS e.cam	Butterworth	LMEGP	0.45 Nyquist	MEW	Chang	128 × 128	3.9

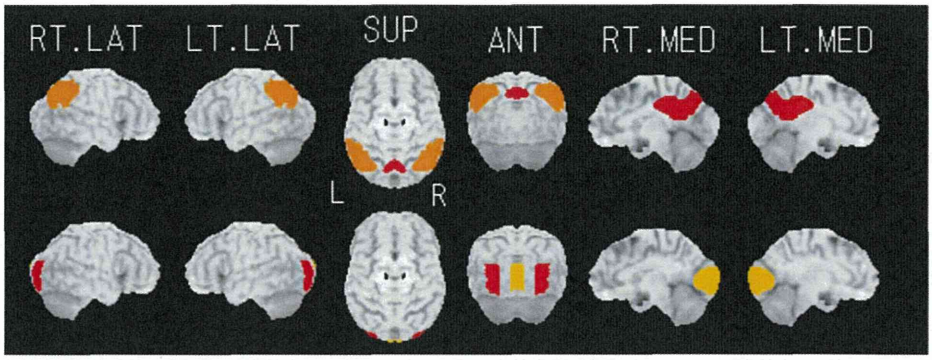

Fig. 1 Template ROI map for AD and DLB patients, which demonstrates significantly lower perfusion in AD patients compared with normal controls and DLB patients. ZSAM used this ROI map (*RT.LAT* right lateral, *LT.LAT* left lateral, *SUP* superior, *INF* inferior, *ANT* anterior, *POST* posterior, *RT.MED* right medial, *LT.MED* left medial)

Table 3 Details of healthy volunteers in NDB

Institution	Number	Age (years) mean ± SD
A	29	64.6 ± 8.4
B	27	63.4 ± 7.1
C	29	64.2 ± 8.2
D	29	64.2 ± 8.2

the normal patients to calculate the *Z*-sum for each ROI. The *Z*-sum of each normal individual was averaged for each ROI to calculate the normal mean and standard deviation of the *Z*-sum. Normal means + 1.64 SD and + 1.96 SD were considered normal *Z*-sum thresholds, and we determined that blood flow was reduced when the *Z*-sum of an analyzed individual exceeded the normal threshold. We used the normal database described by Onishi et al. [7] to prepare normal *Z*-sum thresholds (Table 3).

Clinical adoption of automated system

After preparing *Z*-score images using the normal database described above in which the reconstruction conditions were consistent with the SPECT device, we calculated the *Z*-sum within the template ROIs and compared the SPECT images of patients with the normal *Z*-sum threshold. We compared the ratios (%) of patients with AD and DLB who had reduced blood flow within each ROI. In order to make the best criteria for discriminating AD/DLB from non-AD/DLB, we established two determination criteria for AD/DLB and non-AD/DLB and determined sensitivity, specificity, and diagnostic accuracy rates for each criterion: (1) *Determination of criterion 1 for AD/DLB*. When the *Z*-sum exceeded the normal threshold in one or more of four AD/DLB template ROIs in the bilateral parietal lobe, bilateral posterior cingulate gyrus and precuneus, the patient was assigned to the AD/DLB group. Otherwise, patients were assigned to the non-AD/DLB group; (2) *Determination criterion 2 for AD/DLB*. When the *Z*-sum exceeded the normal threshold in one or more ROIs in the posterior cingulate gyrus and precuneus ROIs, or the *Z*-sum exceeded the normal threshold in two or more of four AD/DLB template ROIs, the patient was assigned to the AD/DLB group. Otherwise, patients were assigned to the non-AD/DLB group.

Diagnostic performance of conventional IMP-SPECT and 3D-SSP Z-score images

We compared automated assessments of conventional IMP-SPECT axial and 3D-SSP *Z*-score images with visual assessments by three experienced nuclear medicine physicians and one neurologist. All of them knew the criteria for abnormalities, but were blinded to the clinical data of the patients. The criteria for AD comprised decreased parietotemporal perfusion compared with sensorimotor perfusion, or obviously decreased posterior cingulate and/or precuneus perfusion compared with sensorimotor perfusion. The criterion for DLB was decreased medial and/or lateral occipital perfusion compared with sensorimotor perfusion. Diagnoses of AD/DLB vs non-AD/DLB based on the conventional IMP-SPECT and 3D-SSP *Z*-score images were classified as follows: definite non-AD/DLB, probable non-AD/DLB, indeterminate, probable AD/DLB and definite AD/DLB.

Visual assessments were evaluated using ROC analysis and AUC were calculated using IBM SPSS statistics. We then compared the diagnostic accuracy between AD/DLB and non-AD/DLB differentiated by visual assessment and ZSAM.

Results

Diagnostic accuracy between AD/DLB and non-AD/DLB differentiated by visual assessment and ZSAM

Table 4 shows the diagnostic accuracy rates of AD/DLB determination criterion 2 at a normal *Z*-sum threshold of the normal mean + 1.64 SD at which specificity between

Table 4 Comparison of the accuracy of visual inspection and ZSAM

Group	Observer	Accuracy		
		Visual inspection	ZSAM	McNemar test
All	A	89.21	83.1	$p = 0.028$
	B	77.34		NS
	C	78.78		NS
	D	70.86		$p = 0.001$
MMSE 24 and more	A	84.75	72.9	NS
	B	55.93		NS
	C	61.02		NS
	D	50.85		$p = 0.007$
MMSE 20–23	A	93.07	84.2	$p = 0.063$
	B	82.18		NS
	C	84.16		NS
	D	76.24		NS

ZSAM's criteria was set as #2 with threshold of mean + 1.64 SD

Table 5 Number of cases exceeding the Z-sum threshold in AD/DLB ROI

	Threshold	
	Mean + 1.64 SD	Mean + 1.96 SD
Parietal ROI[a]		
AD ($n = 202$)	159 (78.7 %)	146 (72.3 %)
DLB ($n = 40$)	33 (82.5 %)	31 (77.5 %)
Posterior cingulate and precuneus ROI[a]		
AD ($n = 202$)	175 (86.6 %)	166 (82.2 %)
DLB ($n = 40$)	32 (80.0 %)	30 (75.0 %)
Occipital ROI		
AD ($n = 202$)	58 (28.7 %)**	50 (24.8 %)**
DLB ($n = 40$)	24 (60 %)*	20 (50 %)**

* $p = 0.0013$, ** $p < 0.0001$ by χ^2 test

[a] There is no significant group difference by χ^2 test

determination by ZSAM and visual inspection was high. The diagnostic accuracy rates did not significantly differ between ZSAM and visual assessments by two of the four raters (McNemar test). One rater had a significantly higher visual diagnostic accuracy rate when all patients and the group with MMSE scores of 20–23 points were included. Another had a significantly higher diagnostic accuracy rate by ZSAM when all patients and those with mild disease were included.

Table 5 shows the ratios (%) of patients with reduced blood flow in the parietal lobe, posterior cingulate gyrus and precuneus and occipital lobe ROIs among 202 patients with AD and 40 patients with DLB. At a normal threshold of mean + 1.64 SD, 78.7 and 82.5 % of patients with AD and DLB, respectively, had reduced blood flow in the parietal lobe ROI, and 86.6 and 80.0 %, respectively, had reduced blood flow in the posterior cingulate gyrus and precuneus ROI. The ratios of patients with AD and DLB and reduced blood flow did not significantly differ. At normal thresholds of mean + 1.64 SD and mean + 1.96 SD, 60.0 and 50.0 % of patients, respectively, with DLB and 28.7 and 24.8 %, respectively, of those with AD had reduced blood flow in the occipital lobe ROI, with DLB being significantly higher for both situations ($p < 0.0001$, $p = 0.013$ χ^2 test).

Figure 2 shows the diagnostic performance of ZSAM (Fig. 2a) and visual assessment (Fig. 2b) for differentiating AD/DLB from non-AD/DLB. The sensitivity of ZSAM based on the AUC for all patients, and those with MMSE scores of ≥24 and 20–23 points was 85.1–93.0 %, 74.0–88.0 % and 88.4–94.2 %, respectively, with 25.0–50.0 %, 33.3–44.4 % and 33.3–60.0 %, specificity, respectively. Diagnostic accuracy rates were 80.6–84.2 %, 69.5–79.7 %, and 82.2–85.1 %, respectively.

The sensitivity of visual assessment by the four raters for all patients, and those with MMSE scores of ≥24 and 20–23 points was 71.1–94.6 %, 46.0–90.0 % and 75.6–96.5 %, respectively with 38.9–69.4 %, 22.2–77.8 % and 53.3–80.0 %, specificity, respectively. Diagnostic accuracy rates were 70.9–89.2 %, 50.6–84.8 % and 76.2–93.1 %, respectively. The AUC in the ROC analyses were 0.74–0.84, 0.66–0.85 and 0.81–0.93, respectively.

Discussion

Differentiation between AD/DLB and non-AD/DLB

Blood flow is reduced in the temporoparietal association area, posterior cingulate gyrus, and precuneus of patients with DLB as in AD, but blood flow in the occipital lobe is lower in DLB [14]. Thus, AD is impossible to differentiate from DLB in the temporoparietal association area, posterior cingulate gyrus and precuneus. To discriminate AD or DLB patients from other disease patients is the first step of differential diagnosis process. Because both in AD and DLB brain, bilateral parietal and posterior cingulate perfusion reduction exists, and in non-AD/DLB brain those regional perfusion reductions exist a minimum. After this process, we can move to discriminate AD from DLB. Therefore, patients with AD/DLB and patients with other degenerative dementias should be initially differentiated using these regions. The present study found that high ratios of patients with AD and DLB had reduced blood flow in the AD/DLB template ROIs (bilateral parietal lobe, posterior cingulate gyrus and precuneus), and that the ratios did not significantly differ. We used SPECT images of AD and normal groups to prepare AD/DLB template ROIs, but

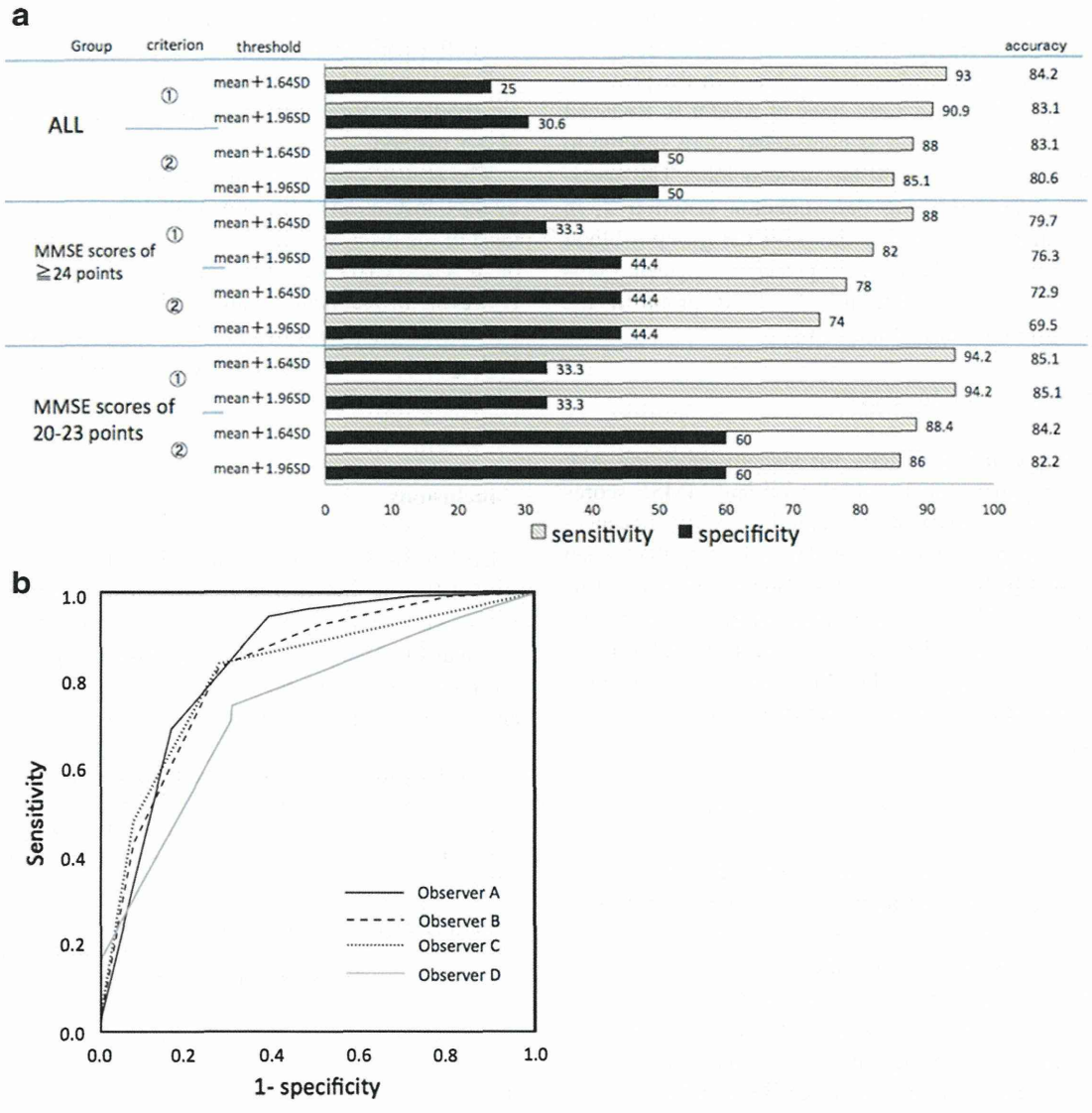

Fig. 2 **a** Graph of sensitivity, specificity and accuracy of differential diagnosis performance of ZSAM comparisons between the AD/DLB group and non-AD/non-DLB. **b** ROC curve of visual inspection of AD/DLB group vs non-AD/non-DLB

not those of the DLB group. We believe that using the ROIs as regions with which to evaluate the reduced blood flow sites characteristic of AD and DLB is not problematic.

Differentiation between AD and DLB

Although significantly more patients with DLB had reduced blood flow in the occipital lobe ROI, the ratio of 60 % was not considered very high, and 28 % of patients with AD had reduced blood flow in the occipital lobe. We assumed that older patients in general tend to have decreased perfusion in the occipital lobe, including those with AD. Because we considered that differentiating between AD and DLB based on reduced blood flow in the occipital lobe ROI was difficult, we differentiated AD/DLB from non-AD/DLB using AD/DLB template ROIs. Differentiation between AD and DLB should be improved by using not only the occipital lobe ROI but also other reference sites or clinical psychological test trials. This is a topic for a future study.

Differentiation by ZSAM

The sensitivity of for detecting AD/DLB using ZSAM was 74–88 % among patients with mild disease and MMSE scores of ≥24 points, and 88.4–94.2 % for those with MMSE scores of 20–23 points, but the specificity was low. Specificity of ZSAM was less than 60 % in contrast with sensitivity more than 70 %. High sensitivity is not useful for ruling in disease, but a high sensitivity test is reliable

when its result is negative, since it rarely misdiagnoses those AD/DLB diseases. Minoshima et al. [15] described that glucose metabolism becomes reduced in the posterior cingulate gyrus from the early stage of AD/DLB. Reduced metabolism and blood flow is considered more specific to AD/DLB at this site than at the parietal lobe. The specificity was improved using determination criterion 2, in which a patient is assigned to the AD/DLB group if blood flow is reduced in the ROI for the posterior cingulate gyrus and precuneus, and to the non-AD/DLB group if the reduction is in the parietal lobe ROI.

Visual differentiation by experts

The sensitivity and specificity for visually detecting AD/DLB among patients with mild disease and MMSE scores of $\geq$24 points was 46.0–90.0 % and 22.2–77.8 %, respectively, indicating greater inter-reader variability than when patients had MMSE scores of 20–23 points. This might be because elder patients with less severe disease have smaller reductions in blood flow and metabolism and do not present typical findings of AD [16], and the raters could not visually determine the significance of the blood flow reduction.

Comparison of visual and ZSAM assessment

One expert rater had significantly higher diagnostic accuracy rates than ZSAM for all patients and those with MMSE scores of 20–23 points (89.2 and 93.1 %, respectively. The diagnostic accuracy rates also did not significantly differ between visual assessment by the other three raters and ZSAM, or the diagnostic accuracy rate by ZSAM was significantly higher. "No significant difference" in a small sample sized study does not mean "really no difference". In order to show real no difference, a power analysis in a larger sample group is required, therefore we may have to increase the number of non-AD/DLB group in our study. In spite of this, evaluations by ZSAM and by expert visual assessment are similarly effective. The results of ZSAM could serve as a diagnostic reference to aid the expert visual interpretation of SPECT images of degenerative dementia.

Limitations

There are some limitations in this study. Because it was impossible to obtain the pathology findings from all the subjects, we had to set the clinical diagnosis as gold standard which has the limitation of diagnostic accuracy: approximately 80 %. Visual inspection of perfusion SPECT for dementia diagnosis does not only depend on the affected regions in the parietal and posterior cingulate cortices but also on the frontal, hippocampal, sensorimotor, cerebellar and other regions. In this study, we focused on only the parietal and posterior cingulate cortices; however, we should analyze other regions for further improvement of our method.

The accuracy of differential diagnosis may be influenced by the constitution of the non-AD/DLB group. In this study most of the diseases were FTD and PSP, but if the numbers of SPA and CBD were large, the results may be different. However, in practical situations the numbers of FTD and PSP are larger than those of SPA and CBD, therefore our findings would not be affected adversely in a clinical situation.

Conclusions

ZSAM using IMP-SPECT and 3D-SSP can differentiate AD/DLB from non-AD/DLB across several institutions, its diagnostic performance is equivalent to that of expert visual assessment, and it might be clinically applicable. We presently use this method as an aid to visual assessment and not as the main diagnostic modality.

Acknowledgments The authors thank Mr. Kiyotaka Watanabe and Mr. Shuya Miki (Nihon Medi-Physics, Tokyo, Japan) for providing and improving the iNEUROSTAT++ program, which uses the 3D-SSP program and was dedicated to this *Z*-score summation analysis method.

Conflict of interest Kazunari Ishii received lecture fees from Nihon Medi-Physics. Kengo Ito, Atsushi Nakanishi, Shin Kitamura, and Akira Terashima declare that they have no conflict of interest.

References

1. Reiman EM, Jagust WJ. Brain imaging in the study of Alzheimer's disease. Neuroimage. 2012;61:505–16.
2. Herholz K. Perfusion SPECT and FDG-PET. Int Psychogeriatr. 2011;23(Suppl 2):S25–31.
3. Ishii K, Kanda T, Uemura T, Miyamoto N, Yoshikawa T, Shimada K, et al. Computer-assisted diagnostic system for neurodegenerative dementia using brain SPECT and 3D-SSP. Eur J Nucl Med Mol Imaging. 2009;36:831–40.
4. Minoshima S, Frey KA, Koeppe RA, Foster NL, Kuhl DE. A diagnostic approach in Alzheimer's disease using three-dimensional stereotactic surface projections of fluorine-18-FDG PET. J Nucl Med. 1995;36:1238–48.
5. McKhann G, Drachman D, Folstein M, Katzman R, Price D, Stadlan E. Clinical diagnosis of Alzheimer's disease: report of the NINCDS-ADRDA Work Group under the auspices of Department of Health and Human Services Task Force on Alzheimer's Disease. Neurology. 1984;34:939–44.
6. McKeith IG, Dickson DW, Lowe J, Emre M, O'Brien JT, Feldman H, et al. Consortium on DLB. Diagnosis and management of dementia with Lewy bodies: third report of the DLB Consortium. Neurology. 2005;65:1863–72.

7. Onishi H, Matsutomo N, Kai Y, Kangai Y, Amijima H, Yamaguchi T. Evaluation of a novel normal database with matched SPECT systems and optimal pre-filter parameters for 3D-SSP. Ann Nucl Med. 2012;26:16–25.
8. Neary D, Snowden JS, Gustafson L, Passant U, Stuss D, Black S. Frontotemporal lobar degeneration: a consensus on clinical diagnostic criteria. Neurology. 1998;51(1):546–54.
9. Litvan I, Agid Y, Calne D, Campbell G, Dubois B, Duvoisin RC, et al. Clinical research criteria for the diagnosis of progressive supranuclear palsy (Steele–Richardson–Olszewski syndrome): report of the NINDSSPSP international workshop. Neurology. 1996;47:1–9.
10. Ishikawa M, Hashimoto M, Kuwana N, Mori E, Miyake H, Wachi A, et al. Guidelines for management of idiopathic normal pressure hydrocephalus. Neurol Med Chir (Tokyo). 2008;48(Suppl):S1–23.
11. Lang AE, Riley DE, Bergeron C. Cortical-basal ganglionic degeneration. In: Calne DB, editor. Neurodegenerative disease. Philadelphia: Saunders; 1994. p. 877–94.
12. Gilman S, Wenning GK, Low PA, Brooks DJ, Mathias CJ, Trojanowski JQ, et al. Second consensus statement on the diagnosis of multiple system atrophy. Neurology. 2008;71:670–6.
13. Calne DB, Snow BJ, Lee C. Criteria for diagnosing Parkinson's disease. Ann Neurol. 1992;32 (Suppl):S125–7.
14. Ishii K, Yamaji S, Kitagaki H, Imamura T, Hirono N, Mori E. Regional cerebral blood flow difference between dementia with Lewy bodies and AD. Neurology. 1999;53:413–6.
15. Minoshima S, Giordani B, Berent S, Frey KA, Foster NL, Kuhl DE. Metabolic reduction in the posterior cingulate cortex in very early Alzheimer's disease. Ann Neurol. 1997;42:85–94.
16. Sakamoto S, Ishii K, Sasaki M, Hosaka K, Mori T, Matsui M, et al. Differences in cerebral metabolic impairment between early and late onset types of Alzheimer's disease. J Neurol Sci. 2002;200:27–32.

Radiol Phys Technol
DOI 10.1007/s12194-015-0311-8

Impact of injected dose and acquisition time on a normal database by use of 3D-SSP in SPECT images: quantitative simulation studies

Hideo Onishi · Jun Hatazawa · Jyoji Nakagawara · Kengo Ito · Sang Kil Ha-Kawa · Yasuhiko Masuda · Keiichi Sugibayashi · Masaaki Takahashi · Kei Kikuchi · Noboru Katsuta

Received: 26 October 2014 / Revised: 23 February 2015 / Accepted: 24 February 2015

Abstract The present study aimed to validate the accuracy of normal databases (NDBs) with respect to variable injected doses and acquisition times by use of three-dimensional stereotactic surface projections (3D-SSP) in *N*-isopropyl-*p*-[123I]-iodoamphetamine (I-123-IMP) brain perfusion images. We constructed NDBs based on brain SPECT images obtained from 29 healthy volunteers. Each NDB was rebuilt under simulated unique conditions by use of dynamic acquisition datasets and comprised injected doses (222, 167, and 111 MBq) and acquisition times (30, 20, and 15 min). We selected seven of 29 datasets derived from the volunteers to simulate patients' data (PD). The simulated PD were designed to include regions of hypoperfusion. The study comprised protocol A (same conditions for PD and NDB) and protocol B (mismatched conditions for PD and NDB). We used 3D-SSP to compare with the *Z* score and detection error. The average *Z* scores were decreased significantly in protocol A [PD (High)–NDB (High) vs. PD (Low)–NDB (Low); PD (30 m)–NDB (30 m) vs. PD (15 m)–NDB (15 m) and PD (20 m)–NDB (20 m)].The average *Z* scores of PD (High) and PD (Medium) with NDB (High) did not differ significantly in protocol B, whereas all others were decreased significantly. The error of detection increased 6.65 % (protocol A) and 32.05 % (protocol B). The *Z* scores were specific to the injected dose and acquisition time used in 3D-SSP studies, and the calculated *Z* scores were affected by mismatched injected doses and acquisition times between PD and selected NDBs.

H. Onishi (✉)
Program in Health and Welfare, Graduate School of Comprehensive Scientific Research, Prefectural University of Hiroshima, 1-1 Gakuenmachi, Mihara, Hiroshima 723-0053, Japan
e-mail: onisi@pu-hiroshima.ac.jp

J. Hatazawa
Department of Nuclear Medicine and Tracer Kinetics, Osaka University Graduate School of Medicine, Osaka, Japan

J. Nakagawara
Department of Neurosurgery Integrative Stroke Imaging Center, National Cerebral and Cardiovascular Center, Suita, Japan

K. Ito
Department of Clinical and Experimental Neuroimaging, Center for Development of Advanced Medicine for Dementia, National Center for Geriatrics and Gerontology, Obu, Japan

S. K. Ha-Kawa
Department of Nuclear Medicine, Kansai Medical University Hirakata Hospital, Hirakata, Japan

Y. Masuda
Division of Radiology, Department of Medical Technology, Asahikawa Red Cross Hospital, Asahikawa, Japan

K. Sugibayashi
Department of Radiology, Kansai Medical University Hirakata Hospital, Hirakata, Japan

M. Takahashi
Department of Radiology, Teishinkai Hospital, Sapporo, Japan

K. Kikuchi
Department of Radiology, Kitasato University Hospital, Sagamihara, Japan

N. Katsuta
Division of Medical Technology, Kumamoto University Hospital, Kumamoto, Japan

Published online: 11 March 2015

Keywords Alzheimer's disease · *Z* score · Three-dimensional stereotactic surface projection · I-123 iodoamphetamine · Early detection

1 Introduction

As the number of patients with Alzheimer's disease (AD) has increased, early diagnosis of AD has received increased focus for both social and medical reasons. Single photon and positron emission tomography (SPECT and PET, respectively) have played important roles as early diagnostic tools in clinical studies and have become popular [1–5]. The statistical voxel-based analysis method also provides good diagnostic support for an early diagnosis of AD [6, 7]. We have developed a fully automated diagnostic system using the NEUROSTAT program, which comprises three-dimensional stereotactic surface projections (3D-SSP) [8]. However, these tools require a database of healthy brain images (NDB). We rebuilt a novel normal perfusion database generated from dynamic brain SPECT images of a large population of healthy individuals [9, 10]. This novel NDB does not take into account variations in injected doses and acquisition times among clinical studies at various institutions. Acquisition time is associated with patient burden, and health insurance limits the amount of injectable doses of radioactivity in Japan. The effects of the *Z* score on various types of compensation [11] have been reported, but the effect of *Z* scores when a normal NDB is mismatched with an injected dose and acquisition time has not been described.

Our aim in this study was to validate the performance and accuracy of a rebuilt NDB with respect to variable injected doses and acquisition times. Data about injected doses and acquisition times were generated and reconstructed from modified dynamic SPECT projection datasets. We simulated patients' data (PD) by constructing hypoperfused regions of the brain with specific volumes and then compared *Z* scores and detection errors with those of the NDB under various conditions.

2 Materials and methods

2.1 Study design

In this study, we used brain SPECT and 3D-SSP to compare the impact of injected doses (222, 167, and 111 MBq) and acquisition times (30, 20 and 15 min) qualitatively on the NDB. Protocol A evaluated the effects when the conditions of the NDB and the simulated PD were the same. Protocol B evaluated the effects when the simulated PD were variable and the NDB was fixed. We assumed that projection data counts were linear during injection of the tracer and acquisition time without a loss of counts. We validated the linearity of the radioactivity concentration and the SPECT counts using a Pai phantom.

2.2 Pai phantom

Figure 1a shows the custom-designed Pai phantom (Shimaya Kiki Co., Ltd. Hiroshima, Japan), which is shaped like a pie-chart, divided into six chambers and symmetrically positioned in a cylinder 100 mm in length with a diameter of 160 mm. Each chamber contained 480 mL of a homogeneous solution of 1.0 (0.016 MBq/mL), 2.0- , 4.0- , 8.0- ,

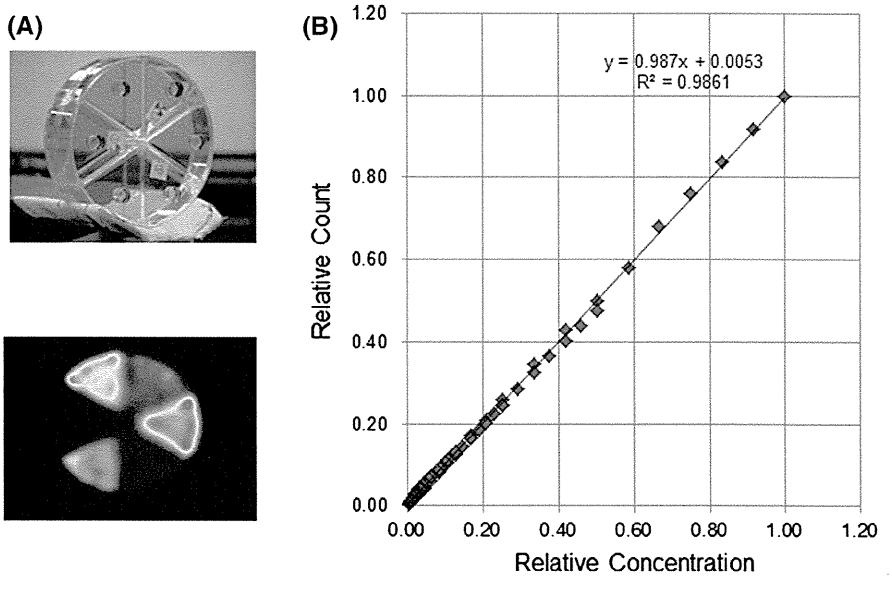

Fig. 1 **a** Pai phantom and reconstructed SPECT image, **b** linear regression analysis shows relationship between relative SPECT counts and relative concentration

16.0- , and 32.0-fold concentrations of ^{123}I. Images were acquired continuously from the Pai phantom by use of a 128 × 128 matrix (pixel size 3.9 mm) over 360° in 4 steps (90 projections) for 12 rotations at 2.5 min/rotation. Procedures for reconstruction, scatter, and attenuation correction of images were the same for normal database sets.

2.3 Participants

We analyzed PD that are described in a previous retrospective study [9]. Twenty-nine healthy volunteers [10 males, 19 females, mean age (±SD), 64.2 ± 8.2*y*; range 52–78*y*] at 8 institutions provided written informed consent to having their data analyzed in the present study. The participants were judged as "normal" based on their medical history, a physical assessment, and brain MRI findings [9], and the Ethics Review Boards of the participating institutions approved the study protocol. The participants were injected intravenously with 222 MBq of *N*-isopropyl-*p*-[123I]-iodoamphetamine (I-123-IMP) (Nihon Medi-Physics, Tokyo, Japan) while resting in the supine position with their eyes closed, and then SPECT data collection from each person was started 15 min later and continued for about 30 min.

2.4 Imaging procedures

We continuously acquired I-123-IMP dynamic SPECT images using an e.com rotating dual-headed gamma camera (Siemens, Malvern, PA, USA) equipped with low-medium energy general purpose collimators (FWHM 10.4 at 10 cm in air) under the following conditions: 128 × 128 matrix (pixel size 3.9 mm) over 360° in 4 steps (90 projections), for 12 rotations at 2.5 min/rotation (total acquisition time 30 min). The SPECT data were processed with use of a Syngo MI Workplace (Siemens). All projection data sets were passed through a Butterworth filter (cutoff frequency 0.58 cycles/cm) [9, 10] and reconstructed with use of a ramp back-projection filter. Scatter was corrected with use of a multi-energy-window, and an attenuation correction was applied by use of the post-reconstruction Chang method (attenuation coefficient 0.146/cm).

2.5 Normal database sets

The NDB sets of injection doses (222, 167, 111 MBq) and acquisition times (30, 20, 15 min) were merged for each continuously acquired rotational projection dataset. We generated NDBs to estimate injected doses of 222, 167, and 111 MBq, respectively, and others to estimate acquisition times from continuous dynamic SPECT data sets (Table 1). We are defined the NDB (High), NDB (Medium), and NDB (Low) to represent NDBs with a 222 MBq injected dose, 167 MBq injected dose, and 111 MBq injected dose, and NDB (15 m), NDB (20 m), NDB (30 m) for NDBs with 15, 20 and 30 min of acquisition time. The NDB (High) and NDB (30 m) were the same.

Table 1 NDB method of merged acquisition rotation data sets by injected dose and acquisition time

Estimated injected dose and acquisition time, NDB	Rotation number (2.5 min/rotation)											
NDB (High)	1	2	3	4	5	6	7	8	9	10	11	12
NDB (Medium)	1	2	3		5	6	7		9	10	11	
NDB (Low)	1		3		5		7		9		11	
NDB (30 m)[a]	1	2	3	4	5	6	7	8	9	10	11	12
NDB (20 m)	1	2	3	4	5	6	7	8				
NDB (15 m)	1	2	3	4	5	6						

Dynamic data sets were obtained from each gamma camera after 12 rotations at 2.5 min per angle of rotation. Projection data sets for each injected dose and acquisition time were generated to merge with the rotation projection datasets (2.5 min/rotation). For example, projection data sets derived from an injected dose of 111 MBq were merged with phase datasets 1, 3, 5, 7, 9, and 11. Projection datasets derived from acquisition times of 20 min from 2.5 min/rotation were similarly merged with phase datasets 1, 2, 3, 4, 5, 6, 7 and 8

[a] NDB (30 m) = NDB (High)

2.6 Simulated patients' data

Data generated from seven healthy volunteers were taken as the basis for simulated patient data (PD). Five PD datasets of injection doses and acquisition times were created under the same conditions as those in the generated NDBs. The PD (High), PD (Medium), and PD (Low) were simulated injection doses of 222, 167, and 111 MBq; PD (30 m), PD (20 m), and PD (15 m) were simulated acquisition times (30, 20, and 15 min) acquired from dynamic SPECT data sets. The SPECT imaging process was the same as that used for generating the NDB. Various regions with perfusion defects were quantified as follows: perfusion defects were simulated in the bilateral posterior cingulate gyrus, precuneus, and cuneus regions. Regions with specified volumes were simulated according to a three-dimensional brain coordinate system based on Level 3 in the anatomic classification of the Talairach Daemon database as described in [9]. Each collection of PD data included hypoperfused regions with a summarized area of 5744 mm^2, and the hypoperfused decrease rate was 70 % relative to the original SPECT count. The projection data (90 projection sets in 128 × 128 matrices) were generated from perfusion defect SPECT datasets by use of an in-house projection generating program. Images were reconstructed by filtered back-projection without a pre-processing filter.

2.7 Evaluation

We analyzed SPECT datasets statistically using FALCCON iSSP 5 Ver. 1.0 software (Nihon Med-Physics Co. Ltd., Tokyo, Japan). Data were quantified and displayed by use of the stereotactic extraction estimation program, SEE Ver. 2.1 (Nihon Med-Physics Co. Ltd., Tokyo, Japan) [11]. Average Z scores were calculated by use of whole-brain values, and they exceeded the Z value threshold. The detection error was determined by use of an in-house program [12].

2.7.1 Linearity of radioactivity concentration and SPECT count

Twenty-nine datasets with differing radioactivity concentrations were computed from the amount of radioactivity and acquired continuously during 12 rotations. ROIs were located on the SPECT images. Average SPECT counts were calculated from circular ROIs with a diameter of 50 mm for each chamber in the merged Pai phantom SPECT data. The linear regression between radioactivity concentrations and averaged SPECT counts was then analyzed.

2.8 Standard deviation histogram of normal database sets

Each NDB set was generated at various injected doses and acquisition times. We created standard deviation (SD) histograms from each pixel in SD images of the NDB, and compared how differences in image acquisition conditions affect the SD of NDBs.

2.9 Z scores and detection error

Average Z scores for a hypoperfused defect in response to variations were assessed in protocol A. We describe combinations of PD and NDB at the same injected doses and acquisition times as PD (High)–NDB (High), respectively.

Average Z scores were also evaluated as a defect response to variations in the PD data on the fixed NDB (High) [PD (Medium)–NDB (High)] in protocol B. We describe different injected doses and acquisition times in the PD combined with a fixed NDB as PD [Low–NDB (High) (PD (20 m)–NDB (30 m)]. We evaluated the detection error between the measured and actual areas of specific hypoperfusion regions. We assessed how changes in the injected doses and acquisition times between the NDB and PD affected the error in detecting hypoperfused areas in protocols A and B.

2.10 Statistical analysis

All data were expressed as mean ± SD. Significant differences between mean Z scores were analyzed by ANOVA, followed by the Tukey–Kramer test. Values with $p < 0.05$ were considered to reflect statistically significant differences. All data were analyzed statistically by use of the SPSS 18.0 (IBM Corp, Chicago, IL, USA).

3 Results

3.1 Linearity of radioactivity concentration and SPECT count

The results of the linear regression analysis of relative SPECT values and the radioactivity concentration were: $y = 0.987x + 0.005$ ($R^2 = 0.98$). The gradient of the regression function was about 1.0 and the y-intercept value was about 0.0 (Fig. 1).

3.2 SPECT counts from simulated patients

Figure 2 shows the SD histogram generated from the NDB at various injected doses and acquisition times. The modes of the SD distribution determined from 3D-SSP increased

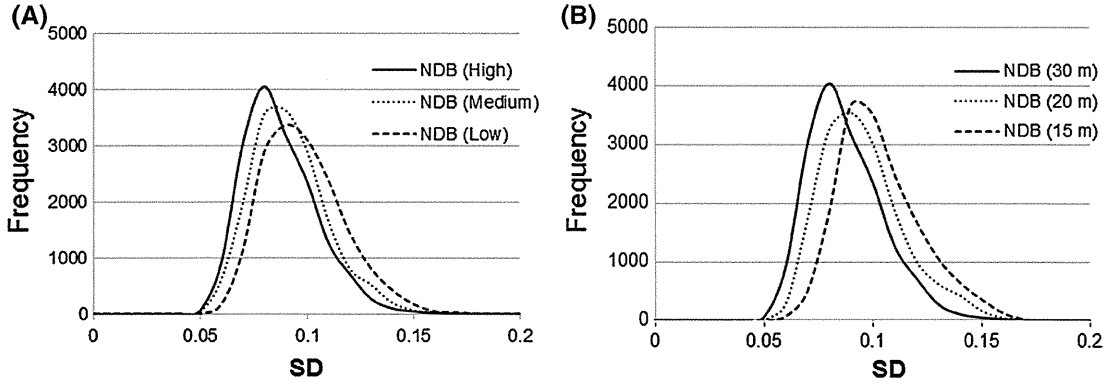

Fig. 2 Histograms of SD obtained at different injected doses (**a**) and acquisition times (**b**) in normal database. The histogram distribution of SD was generated from the SD of each brain pixel of all participants. Horizontal axis, SD score; vertical axis, frequency